BAMS Article

Winter Lightning to the Lee of Lake Ontario: The Lake-Effect Electrification (LEE) Field Campaign

Scott M. Steiger,[a] Eric C. Bruning,[b] Vanna C. Chmielewski,[c] Geoffrey Stano,[d] John Trostel,[e] Kristin M. Calhoun,[c] Kaitlyn R. Jesmonth,[f] Bee Lamsma,[a] Timothy Lang,[g] Shaun Laurinaitis,[h] Jessica Losego,[e] Jacquelyn S. Ringhausen,[i,c] Michael Stock,[i,c] Yonggang Wang,[a] Sean M. Waugh,[c] Stephanie A. Weiss,[b] Thomas Weist,[a] and Thomas White[a]

KEYWORDS:
Lake effects;
Lightning;
Atmospheric electricity;
Cloud microphysics;
Mesoscale systems;
Radars/Radar observations

ABSTRACT: The National Science Foundation–sponsored Lake-Effect Electrification (LEE) field campaign intensive observation periods occurred between November and early February 2022–23 across the eastern Lake Ontario region. Project LEE documented, for the first time, the total lightning and electrical charge structures of lake-effect storms and the associated storm environment using a lightning mapping array (LMA), a mobile dual-polarization X-band radar, and balloon-based soundings that measured vertical profiles of temperature, humidity, wind, electric field, and hydrometeor types. LEE also observed abundant wind turbine-initiated lightning, which is climatologically more likely during the winter. The frequent occurrence of intense lake-effect storms and the proximity of a wind farm with nearly 300 turbines each more than 100 m tall to the lee of Lake Ontario provided an ideal laboratory for this study. The field project involved many undergraduate (>20) and graduate students. Some foreseen and unforeseen challenges included clearing the LMA solar panels of snow and continuous operation in low-sunlight conditions, large sonde balloons prematurely popping due to extremely cold conditions, sonde line breaking, recovering probes in deep snow in heavily forested areas, vehicles getting stuck in the snowpack, and an abnormally dry season for parts of the LEE domain. In spite of these difficulties, a dataset was collected in multiple lake-effect snowstorms (11 observation periods) and one extratropical cyclone snowstorm that clarifies the electrical structure of these systems. A key finding was the existence of a near-surface substantial positive charge layer (1 nC m^{-3}) near the shoreline during lake-effect thunderstorms.

SIGNIFICANCE STATEMENT: Winter lightning is an exciting phenomenon and important to study as man-made objects (e.g., wind turbines) can be more likely to be struck this time of year. We involved over 20 undergraduate students in collecting total lightning, mobile radar, and sounding (e.g., electric field) data in several lake-effect storms. These storms have been known to have substantial electrification and occur many times each winter in a small, consistent region east of Lake Ontario. We analyzed 246 lightning flashes from the main data collection period, and over a third of them were associated with towers. The results from this study will have impacts on our general understanding of electrification in winter and summer storms.

DOI: 10.1175/BAMS-D-23-0176.1
Corresponding author: Scott Steiger, scott.steiger@oswego.edu
Supplemental information related to this paper is available at the Journals Online website: https://doi.org/10.1175/BAMS-D-23-0176.s1.

Manuscript received 12 July 2023, in final form 26 July 2024, accepted 15 August 2024

AFFILIATIONS: [a] Department of Atmospheric and Geological Sciences, State University of New York at Oswego, Oswego, New York; [b] Atmospheric Science Group, Department of Geosciences, Texas Tech University, Lubbock, Texas; [c] NOAA/OAR National Severe Storms Laboratory, Norman, Oklahoma; [d] Information Technology Systems Center, University of Alabama in Huntsville, Huntsville, Alabama; [e] Severe Storms Research Center, Georgia Tech Research Institute, Atlanta, Georgia; [f] Department of Atmospheric Sciences, University of Illinois Urbana–Champaign, Urbana, Illinois; [g] Earth Science Branch, NASA Marshall Space Flight Center, Huntsville, Alabama; [h] School of Meteorology, University of Oklahoma, Norman, Oklahoma; [i] Cooperative Institute for Severe and High-Impact Weather Research and Operations, University of Oklahoma, Norman, Oklahoma

1. Introduction

Thundersnow, or when lightning occurs during a snowfall, strikes both meteorologists and the public with awe. It is one of the most exciting phenomena experienced in nature in part due to its rarity (e.g., see The Weather Channel's Jim Cantore's reaction to thundersnow; https://youtu.be/PdRWGMyeSYY). Lightning can be a useful indicator of storm strength and other potential hazards to life and property (e.g., Stough et al. 2017; Schultz et al. 2011). During a snowstorm, thundersnow can be related to changing snowfall rates because its occurrence is related to the evolving cloud microphysics as more rimed particles like graupel are forming in the cloud (Harkema et al. 2020).

Lake-effect snowstorms produce some of the heaviest snowfall rates in the world (Niziol et al. 1995) and have been known to initiate lightning. Six lake-effect thunderstorms occurred during the <2-month field phase of the Ontario Winter Lake-effect Systems (OWLeS) Project 2013–14 (Kristovich et al. 2017; Steiger et al. 2018). Most lake-effect thunderstorms produce tens of flashes, and early studies show the vast majority of the lightning occurring over or within 10 km of the lake (Moore and Orville 1990; Steiger et al. 2009). Steiger et al. (2018) found a shift in lake-effect lightning farther inland compared to the results of Moore and Orville (1990) and associated nearly half of the observed flashes with man-made objects such as wind turbines. With more turbines under construction worldwide, it is essential to improve our understanding of how lightning interacts with the human-built environment to understand damage risks and possible harm to life.

Lake-effect storms (LeSs) provide an excellent laboratory not only to improve the understanding of tower-initiated lightning but also to understand more generally storm electrification. The mixed-phase regions of lake-effect clouds and their electric fields[1] extend down to the ground, allowing for turbines to interact with these aspects of the clouds and for direct observation of unmelted hydrometeors at the surface. During the 2022–23 Lake-Effect Electrification (LEE) field project, observations of these clouds were made via a suite of instrumentation over and near Lake Ontario.

[1] An electric field is a force per unit charge affecting a nearby charge. Large electric fields exist between oppositely charged regions (±) and can initiate lightning.

2. Scientific objectives, background, and design

LeSs provide excellent opportunities to study electrification, as they can persist for several hours to days over one location and continually develop convective and stratiform clouds. Thus, the overarching goal of Project LEE is to document, for the first time, how the electrical

charge structure in lake-effect precipitation bands develops and initiates lightning. The specific objectives are to 1) place the Project LEE lightning and charge region observations in the context of environmental and cloud microphysical conditions via direct (radiosonde) and indirect [dual-pol Doppler on Wheels (DOW) radar] measurements; 2) analyze lightning flash development associated with nearly 300 turbines and other antennas in the Tug Hill Plateau (the "Tug Hill") region east of Lake Ontario; and 3) compare Project LEE results with other electrified winter storms and numerical modeling. The observations necessary to address these objectives were successfully obtained in harsh, wintry conditions!

a. Electrification. Regardless of season or storm mode, lightning ultimately results from the electrification of whatever hydrometeors are present within the storm. This electrification process is sensitive to the concentrations of different hydrometeor types in addition to the surrounding environment (e.g., Saunders et al. 2006), which has unknown implications in LeSs over the Tug Hill. The most efficient mechanism for cloud electrification is noninductive (NI) charge separation due to rebounding collisions of actively riming hydrometeors (e.g., graupel) and ice crystals in the presence of supercooled liquid water (e.g., Illingworth and Latham 1977; Takahashi 1978; Jayaratne et al. 1983), which means that updraft regions supporting mixed-phase hydrometeors provide ideal conditions for cloud electrification. NI electrification is also hypothesized to occur more slowly between snow and ice crystals without supercooled liquid water (Dye and Bansemer 2019). Both the polarity and magnitude of the net charge separated during collisions vary with the surrounding environment and are theorized to be controlled by the relative vapor diffusional growth rate of each particle (Baker et al. 1987; Emersic and Saunders 2010). While laboratory results vary even for typical NI electrification, as summarized by Saunders et al. (2006), there is general agreement that in warm (>−10°C) or liquid-rich environments graupel gains a net-positive (and ice crystals gain a net negative) charge during a collision, while in cold or liquid-starved environments, the opposite occurs. The pair of particles which have separated charge may be referred to as a "charging pair," and the temperature at which the sign of the charging of the particles reverses is known as the "reversal temperature."

The two NI charging regimes readily explain a "normal tripole" often observed near a thunderstorm updraft due to the differential sedimentation of each particle in a vertical continuum of charging pairs (e.g., Illingworth and Latham 1977; Takahashi 1978). A lower, net-positive charge layer (below the –10°C level) results from graupel interacting with ice at the base of the mixed-phase region in warm areas with an influx of unfrozen water particles. The slower-sedimenting, negatively charged cloud ice from the low-level charging pair contributes to a midlevel net-negative charge layer (from –10° to –30°C layer), with the addition of negatively charged graupel from higher altitudes and colder temperatures with more limited liquid water content. The positively charged ice crystals from the upper charging pair contribute to an upper positive charge layer (above the –30°C level). Significant variations can occur even in typical warm-season thunderstorms (e.g., Bruning et al. 2014), and there are questions about what to expect with limited to no warm cloud depth (>0°C, Williams et al. 2005), differing particle characteristics (e.g., Avila et al. 2005; Glassmeier et al. 2018), or at cold temperatures (e.g., Dye and Bansemer 2019; Luque et al. 2016). The lack of any warm cloud depth makes wintertime LeSs a unique natural laboratory for testing our understanding of electrification.

b. Cold season lightning: Lake-effect and other storms. About five lake-effect thunderstorm events with cloud-to-ground (CG) lightning occur per cool season (September–March) over and downwind of Lake Ontario (Moore and Orville 1990; Steiger et al. 2009; Letcher and Steiger 2010). The lightning hot spots are at the east (downwind) end of the lake and

extend inland ~20 km according to the aforementioned studies. In contrast, the lake-effect lightning observed during the OWLeS field project (December–January 2013–14) was all inland of Lake Ontario (no flashes over the lake). Many of the flashes were associated with wind turbines at the Maple Ridge Wind Farm, which is about 50 km inland over the Tug Hill (Steiger et al. 2018; e.g., see their Fig. 11).

The more electrically active LeSs have environments characterized by deeper boundary layers (up to 4 km) that more commonly occur with long-lake-axis-parallel (LLAP; Steiger et al. 2013) storms versus other LeS morphologies (e.g., multibands that cross the shorter axis of a lake). Steiger et al. (2009) found that the height of the storm equilibrium level relative to the –10°C isotherm can discriminate between LeSs with and without lightning. Most lightning events occurred when the equilibrium level was at least 1 km above the –10°C isotherm, and when that isotherm was higher than 1 km AGL, consistent with Kitagawa and Michimoto (1994) and Takahashi et al. (2019). These conditions support mixed hydrometeor types including graupel and snow.

Studies of coastal Japanese sea-effect storms, which are similar to lake-effect storms, have suggested that there is a tilted dipole electrical charge structure exposing positive charge to the surface that leads to an increase in percent positive CG lightning (Brook et al. 1982; Takahashi et al. 2019). Except for one LeS, which was a rainstorm, Moore and Orville (1990) showed most CG lightning is of positive polarity in these storms (a total of two snow and six rainstorms). In contrast, 80% of the 32 CG strokes during the OWLeS campaign were of negative polarity (all frozen precipitation events). Recently, charge structures have been shown to be more complex than previously thought in the Japanese storms (e.g., a tripole; Takahashi et al. 2019; Zheng et al. 2019).

Winter lightning also occurs in some extratropical cyclones, especially in the comma-head region where heavier precipitation bands form (Market et al. 2006). Elevated instability and resultant convection are the main causes of this lightning (Rauber et al. 2014). Lightning is not typically associated with the heaviest snowfall rates in these storms, instead occurring downwind of reflectivity cores (Market and Becker 2009; Harkema et al. 2020).

c. Tower-initiated lightning. Tall towers (>100 m AGL) frequently act either as the initiation point for lightning or as the attachment point for lightning initiated elsewhere in the storm. Due to lower-altitude cloud-base heights and charge regions in winter, locations with tall towers have a greater increase in CG lightning with respect to the surrounding area during winter compared to those same locations in spring and summer seasons (Kingfield et al. 2017). Commonly, tall towers provide a likely connection point for lightning channels. However, with lower cloud bases and falling snow, these towers also provide the impetus for upward-triggered lightning either through local enhancement caused by nearby ongoing lightning or as self-initiated upward lightning (Warner et al. 2012; Stucke et al. 2023). Wind turbines may be particularly effective in allowing for the initiation of upward lightning due to the consistent movement of the blades clearing corona from the blade end (Wang et al. 2008; Montanyà et al. 2014). Due to the presence of wind farms consisting of nearly 300 turbines, the Tug Hill provides an excellent location to study how both electrification and lightning activity in LeSs evolve as convective elements associated with them move inland and over the plateau.

d. Experimental design. The LEE field project occurred from 1 September 2022 to 31 March 2023 over the eastern Lake Ontario region (Fig. 1), with the intensive observation periods (IOPs) focused on the 10 November 2022–4 February 2023 time frame. During this time, a lightning mapping array (LMA) composed of sensors from the Georgia Tech Research Institute (GTRI) and the National Severe Storms Laboratory (NSSL), a DOW mobile dual-polarization

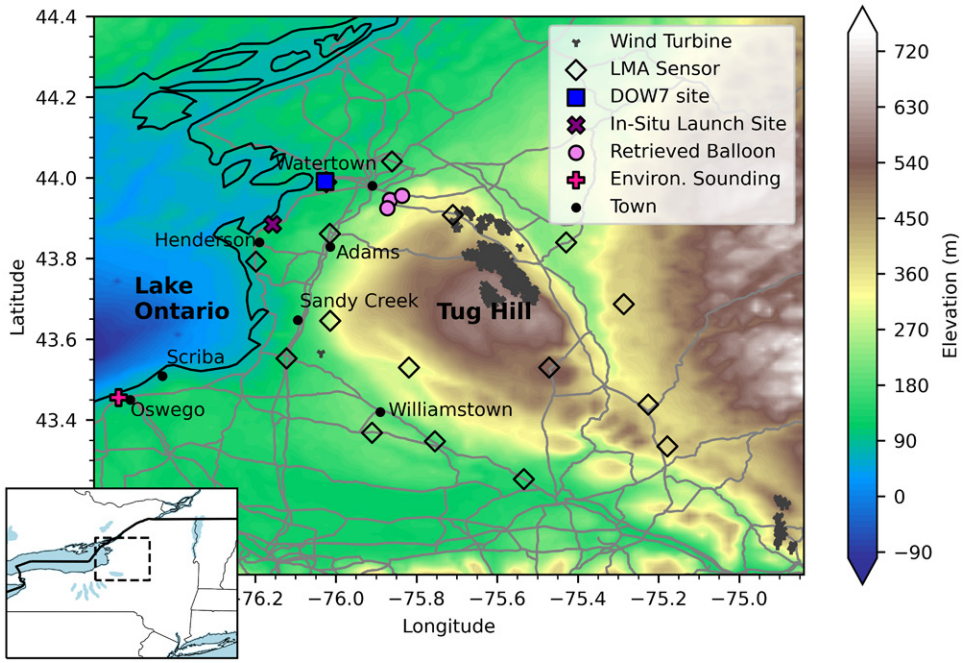

Fig. 1. Example deployment of assets in study domain (dashed rectangle in inset map) during IOP2 (18–19 Nov 2022): LMA sensors, DOW7, and in situ (EFMs with radiosondes, into LeSs) sounding launch and recovery sites and environmental (radiosonde only outside of LeSs) sounding site. Additional sites mentioned in the text are labeled. Note that the DOW7 site was collocated with an LMA sensor site for this IOP. The eastern portion of Lake Ontario (blue) and its elevation (Smith and Sandwell 1997) are shown along with wind turbine locations (Hoen et al. 2018) on the Tug Hill. Primary and secondary roads are also shown (U.S. Census Bureau 2019).

X-band Doppler radar (DOW7), several sounding systems (to measure vertical profiles of temperature, humidity, wind, electric field, and particle imagery), and surface weather observers (located with DOW7 and sonde teams) with instruments to measure snowfall, liquid equivalent, and the ability to photograph hydrometeors were deployed (see Table 1 for more in-depth descriptions, Fig. 1 for facility setup locations, and Fig. 2 for a photo array of these instruments). The LMA is capable of mapping out a flash in space and time as a series of points or "sources" (e.g., see Schultz et al. 2018). The DOW7 scanning strategies varied per IOP including range–height indicator (RHI) scans typically from 0° to 50° elevation at

Table 1. Major observational platforms deployed during the LEE field project.

Platform/instrument	Owner/operator	Location	Reference
LMA–GTRI (eight sensors)	GTRI	Various across the Tug Hill (see Fig. 1)	
LMA–NSSL (8)	NSSL	Various across the Tug Hill (see Fig. 1)	Chmielewski et al. (2023)
DOW7	NSF facility, University of Illinois	Mobile	Wurman et al. (2021)
Radiosonde sounding system (*T*, RH, and wind)—Vaisala	Five separate units: NSSL (4) and SUNY Oswego (1)	NSSL: mobile; SUNY Oswego: on campus (see Fig. 1—environmental sounding)	
Sounding system (*T*, RH, and wind)—iMet	SUNY Oswego	SUNY Oswego campus (Fig. 1)	
Electric field meter (EFM)	NSSL	Mobile, launched with Vaisala sonde	MacGorman and Rust (1998), chapter 6; MacGorman et al. (2008)
Particle Size, Image, and Velocity (PASIV) probe	NSSL	Mobile, launched with Vaisala sonde	Waugh et al. (2015)

Fig. 2. Photos of instruments deployed in the LEE IOP domain (Fig. 1), including DOW7 on (center) 20 Nov 2022 (photo: J. Aikins, University of Illinois) and (upper right) DOW7 on 18 Nov 2022 (photo: J. Aikins); (upper left) the balloon sounding system on 24 Jan 2023 (photo: E. Caldon, SUNY Oswego) and (bottom center) the balloon sounding system on 1 Feb 2023 (photo: S. Steiger, SUNY Oswego); (bottom left) an LMA unit covered in snow (photo: S. Waugh, NSSL) and then (bottom right) an LMA unit cleared on 2 Feb 2023 (photo: S. Waugh).

specified azimuths toward the snowband or other measurement locations, interspersed with regular 89° elevation scans for calibration, and surveillance or plan position indicator (PPI) scans at elevation angles ranging from 0.5° to 3°, as conditions allowed.

Since one of the main project objectives was to study the electrification of lake-effect storms interacting with wind turbines, the LMA was designed for optimal performance (high detection efficiency and location accuracy) over the Tug Hill (Fig. 1). After virtually scouting for potential sites with suspected good field of view, low radio frequency noise, access, and suitable positions for LMA sensors, personnel from the NSSL, University of Oklahoma, and GTRI collaborated on reaching out to potential LMA hosts throughout the region. Access was a priority since we expected to need to clear snow from the sensors throughout the season. The Chmielewski and Bruning (2016) simulation tool was used to optimize sensor spacing and placement, which was especially helpful as the terrain, dense vegetation, and road networks (Fig. 1) limited feasible locations for LMA installations. GTRI sensors were installed earlier in the fall season (September 2022) at locations scattered around the Tug Hill and were expected to result in reasonable solutions of lightning channel location by themselves. While scouting for LMA locations, potential sites for the in situ balloon launches were also evaluated. Sites were required to have space for crews to pull vehicles off main roads, clearance for a balloon and instruments to clear trees or other low obstacles in high winds (>20 m s^{-1}), and be in areas where typical winds during lake-effect events would allow the balloon to ascend over the cloud and a parachute to carry the instruments back down over regions accessible for retrieval [the electric field meter (EFM) and Particle Size, Image, and Velocity (PASIV) were then refurbished and reused in future IOPs]. Over the Tug Hill, any location is only a few kilometers from a road or snowmobile path (though oftentimes roads are not maintained/snowplowed), but there are significantly more remote locations in the Adirondack Mountains to the east to be avoided in high winds.

DOW locations were also chosen over/near the Tug Hill to be able to capture vertical cross sections (RHI scans) along the band toward and away from the lake. For example, the DOW7 location shown in Fig. 1 was placed to sample a west-southwest-to-east-northeast-oriented snowband.

3. Field operations and overview of initial results

Each LEE IOP represented the culmination of planning and collaboration at multiple time scales. The team held daily briefings led by the principal investigators (PIs) on a rotating, weekly basis. These briefings focused on instrument status and maintenance, short- and long-term forecasts, and decision-making to initiate an IOP. The key decision points for an IOP occurred at 96, 48, and 24 h prior to the IOP. At 96-h out, the team went on standby for an event and ensured that all instrumentation was in working order. By 48-h out, with the aid of the first convection-allowing numerical model runs (e.g., NCEP's NAM Nest), the "go" or "no go" decision was made. With a go decision, the final 24 h before the event focused on assigning student roles, determining the final timing and event location, and determining the specific deployment locations for the instrument teams. Once the IOP was underway, it was the responsibility of the weekly, rotating PI lead to focus on nowcasting, determine whether instrument teams had to move, and call an end to the IOP. Following the IOP, the instrument teams would conduct postevent maintenance as well as recover the launched EFM and PASIV instruments.

Eleven IOPs (when GTRI+NSSL LMA, DOW7, sounding, and snow teams deployed) occurred during the 2022–23 Project LEE field campaign (Table 2). Additional rawinsonde and LMA

Table 2. Time period, number of manually identified lightning flashes using LMA data (minimum five sources per flash), number of CG flashes per the ENTLN (Zhu et al. 2022), number of LMA flashes associated with towers (first VHF source within 300 m of a tower and source within 100 m of a tower in parentheses), and number of EFM launches for each LEE IOP and other cold season lightning events (non-IOPs) during the IOP potential time period (10 Nov 2022–4 Feb 2023). Note the NSSL LMA was not in operation for IOP11.

IOP or event	Time period	No. of flashes (LMA)	No. of CG flashes (ENTLN)	No. of confirmed tower flashes	No. of EFM launches
IOP1	0930–1700 UTC 13 Nov 2022	0	0	0	1
Event 1	0800–1600 UTC 17 Nov	11	2	0	0
Event 2	0800–1600 UTC 18 Nov	26	12	4 (1)	0
IOP2	1830 UTC 18 Nov–0630 UTC 19 Nov	9	1	1 (1)	3
Event 3	0630 UTC 19 Nov–1000 UTC 20 Nov	39	26	23 (9)	0
IOP3	1000–2300 UTC 20 Nov	58	31	31 (7)	0
Event 4	0200–0800 UTC 1 Dec	43	7	16 (2)	0
IOP4	2300 UTC 17 Dec–1530 UTC 18 Dec	0	0	0	2
Event 5	1530 UTC 18 Dec–1000 UTC 19 Dec	21	4	6 (1)	0
IOP5	1000–1800 UTC 19 Dec	0	0	0	1
Event 6	1600–1800 UTC 23 Dec	4	3	1 (0)	0
IOP6	1530–2200 UTC 24 Jan 2023	0	0	0	1
Event 7	1900 UTC 25 Jan–0000 UTC 26 Jan	28	24	0	0
IOP7	0500–0730 UTC 27 Jan	0	0	0	0
Event 8	1200–1430 UTC 28 Jan	2	0	0	0
IOP8	1430–1730 UTC 28 Jan	0	0	0	2
IOP9	0500–1030 UTC 31 Jan	0	0	0	0
IOP10	1030 UTC 1 Feb–0030 UTC 2 Feb	0	0	0	2
IOP11	2200 UTC 2 Feb–0330 UTC 3 Feb	5[a]	11	0	1

[a] The number of flashes indicates this number is highly uncertain due to lower detection efficiency with fewer available LMA sensors. The DOW7 team for this IOP visibly observed 20 flashes.

observations were also collected during other lake-effect events both during the IOP time frame and outside the IOP time frame in September 2022 and March 2023. One environmental rawinsonde was launched from Oswego, New York, during a lake-effect rain event on 1 September 2022, which produced lightning per National Lightning Detection Network (NLDN) observations (Murphy et al. 2021). The GTRI LMA was operating, and two Oswego sondes were launched, during a heavy lake-effect rainstorm on 27–28 September 2022 (which had at least 33 LMA flashes and caused flooding). Last, two Oswego sondes were launched and surface precipitation observations were collected during a nonlightning (per the GTRI LMA) LeS on 19 March 2023.

The winter of 2022–23 had the record lowest seasonal snowfall for Oswego, New York, since 1926, receiving about one-third of the climatological mean of 356 cm (140.1 in.) (NCEI 2023). Nonetheless, Project LEE was able to sample intense LeSs, especially during November. IOP2 and IOP3 and surrounding events 1, 2, and 3 were almost ideal storms to sample in terms of electrification and, at times, interactions with wind turbines. Events 4, 5, and 8 were also LeSs, while events 6 and 7 had lightning associated with extratropical cyclones. The IOPs with no lightning (1 and 4–10) are useful null cases. IOP11 was an excellent case of a lake-effect precipitation band interacting with an Arctic front when lightning occurred.

Overall, there were 246 LMA flashes associated with frozen precipitation events across the eastern Lake Ontario region during the Project LEE IOP potential time frame between early November 2022 and early February 2023 (Table 2). Figure 3 shows the LMA flash extent density for all of the events described in Table 2. The maximum density (~2.5 flash segments km^{-2}) is over the wind turbine fields east of Lake Ontario. About 33% (82/246) of these flashes initiated within 300 m of towers (e.g., wind turbine fields shown in Fig. 3; Table 2). We chose 300 m as a cutoff distance from these objects to be consistent with Steiger et al. (2018), although this likely results in an underestimate of the LMA flashes originating at towers. More lightning channel propagation may be necessary for some of these tower-initiated flashes before the LMA can map the flash, because each LMA station is limited by line of sight and background VHF emissions, resulting in limited overall detection efficiency of VHF sources at low elevations near the towers themselves, particularly in weakly emitting positive leader breakdown. Operational lightning networks [NLDN and Earth Networks Total Lightning Network (ENTLN)] do not map channel paths but do not have the same limitations near ground and are optimized to detect events producing large impulsive currents to the ground or tower, although they may also not observe the initial continuing current produced by upward flash development. About 9% (21/246) of the flashes initiated within 100 m of these towers. However, there were substantial periods

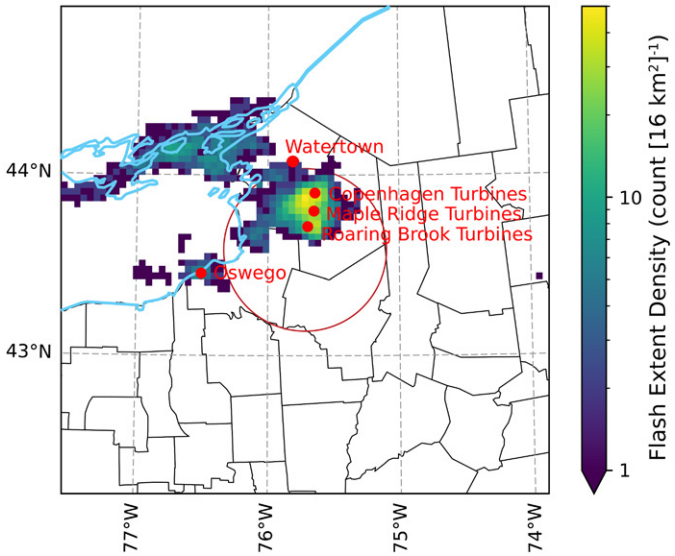

Fig. 3. Map of LMA lightning flash extent density for all of the events during the LEE IOP potential period (November 2022–February 2023). Pertinent locations are identified in red. Each pixel in the color-shaded data is 4 km, and the red ring extends to 50-km range from the center of the LMA (43.586°N, 75.717°W). The map shows counties in New York (black lines) and Lake Ontario and the Saint Lawrence River (blue lines). Light dashed gray lines indicate constant longitude and latitude.

when the lake-effect bands were not over the wind turbine fields shown in Fig. 3. The event immediately prior to and during IOP3 had the most association of lightning with towers, as 56% of this lightning initiated within 300 m of the towers. The lightning over northeast Lake Ontario in Fig. 3 was mostly associated with event 7 and located near a known Canadian wind farm, while the lightning over Oswego, New York, mainly occurred during the latter portions of IOP3 (during which a natural gas power-producing station stack was struck by lightning; see the video in the online supplemental material). In subsequent sections, we report early science highlights from operations during the campaign.

Collaboration with Project IMPACTS. The 2023 campaign of the Investigation of Microphysics and Precipitation for Atlantic Coast-Threatening Snowstorms (IMPACTS) partially overlapped with Project LEE. The IMPACTS focus was observing heavy snowbands in winter extratropical cyclones with the remote sensing ER-2 and the in situ P-3 NASA aircraft (McMurdie et al. 2022), which contrasts with LEE's focus on primarily LeSs. Despite these differences, LEE coordinated successfully with IMPACTS on four flights: 13, 19–20, 25–26, and 29 January 2023. All of these flights featured significant frontal precipitation (either liquid or frozen) in the LEE domain. The ER-2 and P-3 flew near or within the LEE domain, and LEE launched a single rawinsonde per mission when the aircraft were nearby. In this way, LEE served to complement the extensive fixed and mobile ground-based observing network employed by IMPACTS, while IMPACTS provided detailed airborne remote sensing (including electric field measurements above cloud top) and in situ observations of snowband structure that were relevant to LEE, even though they were not of lake-effect snowbands. Lightning was observed with winter precipitation by the LEE LMA during the 25 January 2023 cyclone passage observed by IMPACTS.

4. Initial results from selected IOPs

a. Lake-effect lightning in IOP2 and IOP3. Five days after the first LEE IOP, a trough passage provided favorable winds and a supportive atmospheric boundary layer for a multiday period with electrified LeS east of Lake Ontario (Table 2; events 1–3; IOP2–IOP3). An LeS began on 17 November 2022 over the Oswego area, south of the Tug Hill, with lightning observed visually locally in Oswego as well as by the *GOES-16* Geostationary Lightning Mapper (GLM; Goodman et al. 2013) and the LMA (event 1). The LeS reformed north of the Tug Hill and Watertown, New York, overnight as the trough progression shifted winds southwestward, with lightning reported by the LMA as early as 0800 UTC 18 November (event 2). IOP2 targeted the band as it was coming onshore on the northern edge of the Tug Hill and potentially interacting with the wind farms downstream. The DOW7 was deployed (location in Fig. 1) to the Watertown Airport, taking PPI and RHI scans aligned with the band (Figs. 4b,c) by 1830 UTC. The in situ balloon crew was stationed northeast of Henderson, New York, shortly thereafter (Fig. 1). Three EFM launches (Fig. 4a) were successful—the first at 2258 UTC outside of the updraft and north of the primary band, the second at 0139 UTC 19 November into the primary band, and the third at 0252 UTC into the primary band shortly before it shifted back to the south. In all three EFM launches, relative humidity was near 100% from the surface, with no clear indication of cloud base.

Our preliminary EFM processing was somewhat noisy, though accurate for signed amplitude and trend of electric field E over kilometer-scale depths, so Fig. 4a shows a hand-analyzed version of the significant changes in E, most of which were in the vertical component E_z. Application of a 1D approximation to Gauss's law (Schuur et al. 1991; charge density $\rho \simeq \epsilon\, \Delta E_z/\Delta z$) shows three charge layers (+/−/+) between the surface and 4.3-km altitude. Maximum $|E|$ varied, in part due to whether the balloon was launched precisely into deeper convective cells moving onshore. An $|E| > 100\,\text{kV m}^{-1}$ was observed

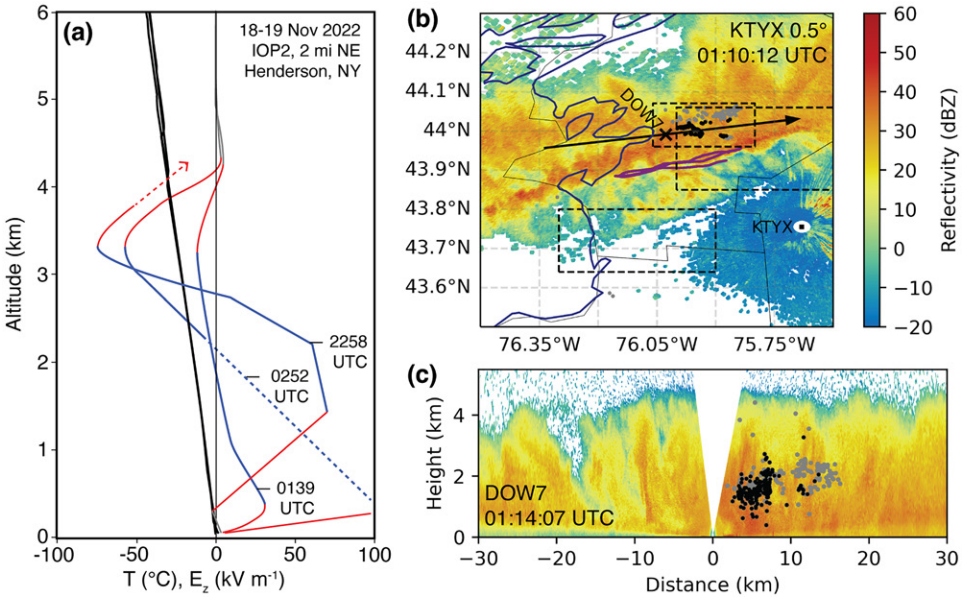

FIG. 4. Radar, lightning, and electric field observations from IOP2, 18–19 Nov 2022. (a) Vertical profiles of temperature (thick black lines) and a manually smoothed, signed magnitude of the electric field $E \simeq E_z$ (red and blue lines), for each of three soundings launched at 2258, 0139, and 0252 UTC, about 2-mi northeast of Henderson, New York (location shown in Fig. 1). 0°C and 0 kV m^{-1} are indicated by a thin vertical black line. Charge layers (sign and magnitude proportional to $\Delta E_z/\Delta z$) are shown in red (positive) and blue (negative). The dashed red line in the 2258 UTC flight indicates noisy and uncertain observations as E returned to zero. The maximum electric field exceeded +100 kV m^{-1} in the 0252 UTC flight, but was clipped, with additional processing uncertainty indicated by the dashed blue line interpolating between the large positive value and the next good value above it. (b) Plan view of S-band radar reflectivity from KTYX NEXRAD at 0.5° elevation angle. The map shows counties in New York (black lines) and Lake Ontario (blue line). Dashed rectangles indicate the locations of flashes in Fig. 5, and purple lines indicate the trajectories of the three balloon launches; time offsets make the radar not representative of all three. (c) Vertical cross section of X-band radar reflectivity from DOW7, with the radar at the x in (b) (height radar relative). Black arrow in (b) indicates the azimuth and increasing distance of the cross section in (c). Dots in (b) and (c) indicate LMA sources (reported by a minimum of six stations and with a location uncertainty measure $\chi^2 = 1.0$) from a flash at 0114:58.6 UTC (also in Figs. 5e–h). Black dots are within 2.5 km of the RHI plane.

in the third launch, just above a very dense charge layer (>+1 nC m^{-3}, inferred from a 1D approximation to Gauss's law; Schuur et al. 1991) extending only 500 m above the surface but already within the cloud, and about a third of the depth of lower positive charge observed in the first flight.

Echo tops via DOW7 (Fig. 4c) and the maximum height of in situ dewpoint saturation were both approximately 5 km. DOW7 observations continued until 0630 UTC 19 November. During these operations, 7.2 in. (18.3 cm) of snowfall was measured at the DOW7 deployment site (1940 UTC 18 November–0640 UTC 19 November) and 3.6 in. (9.1 cm) at the EFM launch site (2008 UTC 18 November–0219 UTC 19 November). The PASIV launches, which were prepped and ready alongside the second and third EFM launches, were aborted due to balloon failures to prioritize the EFM soundings. An issue with the environmental sounding system in Oswego, New York, resulted in the launch only reaching 700 hPa.

During the IOP, lightning was reported by the LMA, GLM, and participants in the field after 2200 UTC 18 November and until 0500 UTC 19 November. A nearshore flash (Figs. 5a–d), an uncommon type during LEE, clearly confirms positive storm charge at ~4-km altitude through traditional analysis of the VHF source characteristics as negative leaders into positive charge regions propagate faster and produce denser, higher-power VHF sources than positive leaders into negative charge regions (e.g., Coleman et al. 2003; Rust et al. 2005). This reflects the altitude of positive charge also seen in the EFM data

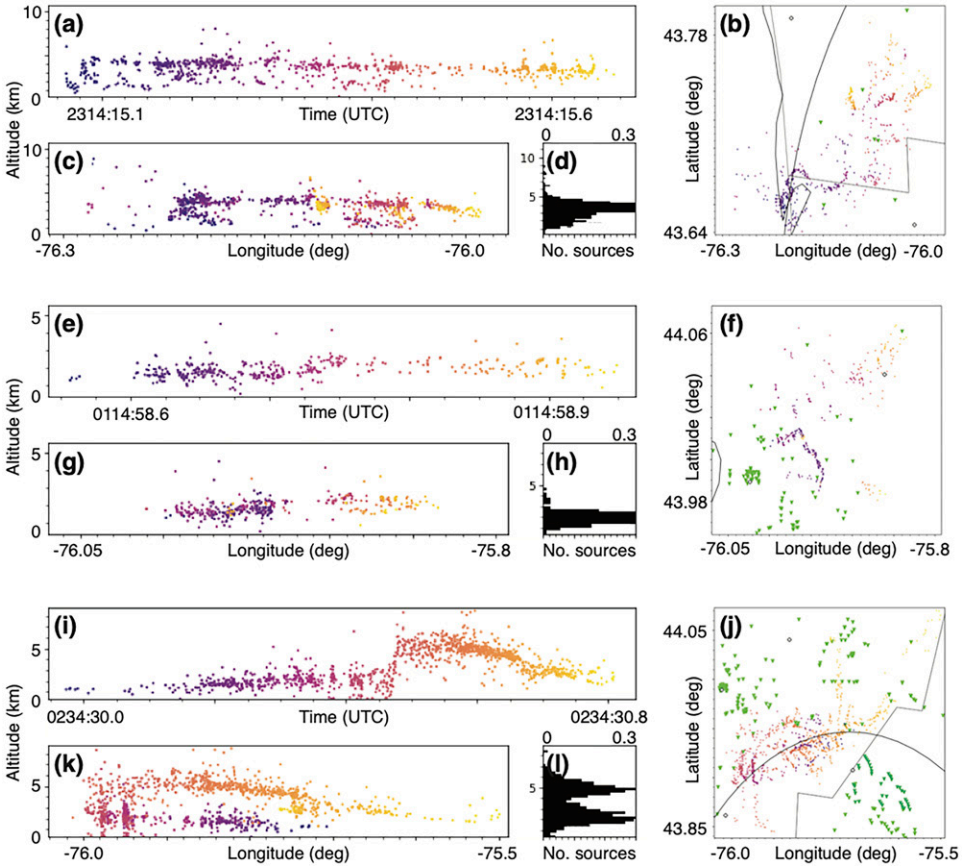

FIG. 5. LMA observations from IOP2 on 18–19 Nov 2022. (a)–(d) A flash near the lakeshore at Sandy Creek, New York (locations shown in Fig. 1), at 2314:15 UTC. (e)–(h) A flash west of Watertown, New York, at 0114:58 UTC. (i)–(l) A flash south and southeast of Watertown, New York, at 0234:30 UTC. LMA panels show VHF source points colored by time. (a),(e),(i) Time–height. (b),(f),(j) Plan view with green dots for man-made tower locations. (c),(g),(k) East-altitude projections. Colors progress from cool to warm with time, as indicated by the times in (a), (e), and (i) for each flash. (d),(h),(l) A normalized VHF source altitude histogram. All altitudes MSL unless otherwise noted. The curved line in (b) and (j) is a 40-km-range ring from the center of the LMA.

and likewise negative charge below at 2–3 km. It is also likely that the lightning traveled through lower positive charge, consistent with the initial downward development, shown by the negative slope of the initial points in the time–altitude plot (Fig. 5a) and negative intracloud events reported at the beginning of this flash by the ENTLN. A second flash, and the most common type observed during the campaign (Figs. 5e–h and with radar in Figs. 4b,c), shows typical LMA data for tower-initiated discharges, with only an upward positive channel into negative storm charge at ~2-km altitude and no evidence of negative channels into positive charge as would occur with bidirectional breakdown within the cloud. A third tower flash (Figs. 5i–l) begins like the second but is followed by secondary upward development on the western side just after 0234:30.4 UTC (Figs. 5i,k) of a negative channel into positive storm charge above 3 km (Figs. 5i–l).

Following the overall successful data collection effort of IOP2, the LeS band continued to produce snow and lightning around the Tug Hill intermittently over the following 40 h (event 3, IOP3). Each of the EFMs launched in IOP2 landed southeast of Watertown (Fig. 1), two of which were successfully recovered prior to IOP3, even though over 1 m of snow had fallen between the instrument landing and the recovery efforts. The third was recovered after snowmelt and before IOP4. The final data collection effort of the ongoing LeS (IOP3) began at 1000 UTC 20 November to sample the ongoing band again after it moved south across the Tug Hill. DOW7 was deployed at Williamstown, New York (~50 km east of Oswego), and the in situ sounding

crews remained stationed on the east side of Oswego. The band reached Oswego at 1440 UTC, again with echo tops near 5 km. Three in situ launches were attempted but unfortunately failed for reasons detailed in the "Operations and logistical challenges" sidebar. No environmental sounding was conducted at Oswego. Large graupel [0.75 in. (1.91 cm) diameter] was observed at the in situ sounding site, much larger than had been observed during IOP2, and ground-level measurements were taken with the PASIV. Lightning was observed by the LMA until 2200 UTC, and DOW7 continued to sample the LeS for another hour. This additional electrically active and remotely sampled case during the IOP2–IOP3 synoptic trough passage can be studied in future research.

b. IOP4–IOP5: No lightning. Another trough expected to be supportive of electrified LeS occurred on 17–19 December 2022 (IOP4–IOP5, event 5). There was significant forecast uncertainty on both the timing of when LeS might be over the target domain on the north side of the Tug Hill and when instability and the boundary layer might best support electrification due to their respective dependencies on the embedded shortwave evolution. Disorganized LeS began in the area on 17 December, and the best conditions for electrification were forecasted to occur on each of 18 (IOP4) and 19 (IOP5) December around 0600 UTC, so an IOP was planned for each day. Crews had 14 of 16 LMA sensors operating, four EFM and one PASIV balloon train, and the environmental sounding system and DOW7 ready to go for the storm system.

Operations and logistical challenges

One of the biggest challenges of LEE, like many field campaigns, was the logistics of operating in difficult lake-effect snow conditions. While these challenges were overcome during the project, it is worth noting examples of what to expect for future projects.

The Project LEE goal of launching large latex balloons in harsh, prolonged cold environments ultimately led to a high rate of popped balloons. The launch tube would become increasingly stiff due to temperature and snow accumulation, making the tube sharp and likely to rupture the balloon. A higher rate of success was achieved by keeping the balloons inside the heated vehicles until inflation and minimizing launch tube contact with the cold, snowy ground. Another possible solution could be using a polyethylene balloon which is less susceptible to rupture, though admittedly about 10× the cost. Wind-blown large graupel (e.g., IOP3; Fig. SB1) also may have caused some balloon failures when their sometimes sharp edges impacted the already fragile, cold balloon.

LEE faced major supply chain shortages due to the COVID-19 pandemic that either significantly delayed or entirely eliminated various components needed for balloon-borne observations. In particular, parts for additional PASIV systems were delayed until nearly the end of the project, reducing the opportunity for data collection. Additionally, the delays impacted iterative testing of a new, consolidated balloon cut-down and instrument let-down package and incorporation of a total water sensor. Unsurprisingly, some issues occurred due to the prolonged cold temperatures, including battery failure, line breaks and tangles, and a loss of tracking information. Furthermore, the pandemic-induced backlog of field projects placed LEE in the middle of a 1.5-yr period of nearly continuous field efforts for some members of the team, further complicating preparations. Nevertheless, several launches of instruments were achieved.

After flight, the balloon-borne instruments had to be collected in regions often covered in considerable snow depth. This made reaching the instruments difficult (hazardous road conditions and nonmaintained roads). While some of the instruments could be reached by vehicle, several required snowshoeing a considerable distance (up to 5 km) or the use of a snowmobile. Sometimes the instruments were buried under more than a meter of snow and took considerable effort to find, even with GPS locators. Sometimes these instruments landed in trees, and a local team of tree climbers retrieved them. Despite these challenges, all instruments launched were successfully recovered and all but one were repaired.

The LMA units were also often covered in snow. One of the most significant challenges occurred in between IOP10 and IOP11 when the NSSL LMAs needed to be retrieved for another project and before an Arctic air mass would have made conditions too dangerous. Some of these units were already encased in several centimeters of ice, but all were retrieved in one day! Earlier in the field project, some of the LMA units and the environmental sonde ground station closer to the lake were also blown over by strong winds.

For IOP4, the DOW7 team operated east of Adams (Fig. 1) by 0000 UTC 18 December, scanning primarily to the west and east to monitor the evolving situation (Figs. 6b,c). The ballooning crew was in position west of DOW7 by 0300 UTC. There were an initial EFM launch at 0356 UTC (Fig. 6a) into the band before it shifted north and a corresponding 0400 UTC environmental sounding in Oswego (not shown). Each of the measurements suggests limited storm depths at the time: The environmental boundary layer sampled in Oswego was only up to 700 hPa; the height of the inversion sampled by the in situ EFM launch was 3.2 km MSL (Fig. 6a); and the echo tops sampled by the DOW7 scans were between 2 and 3 km (Fig. 6c). As in IOP2, the EFM data showed a +/−/+ charge structure but now all within the lowest 1.3 km. The band unexpectedly stalled north of the observation axis for most of the overnight hours, shifting back south in the morning. The in situ crew launched an EFM and PASIV sounding pair at 1253 and 1256 UTC, respectively, and the Oswego team provided another environmental sounding at 1300 UTC. The DOW7 team continued operations until 1530 UTC, and little change was observed in the band depth. No lightning flashes were observed throughout the IOP, making IOP4 a null case. However, lightning flashes were observed shortly after the end of the IOP over the Tug Hill starting after 2000 UTC as the band moved south (event 5).

A secondary attempt was made to sample the band as it crossed to the southern side of the Tug Hill and weakened (IOP5). DOW7 was deployed to Williamstown, New York, and began scanning shortly after 1000 UTC 19 December, doing RHI scans initially north and east into the band and then west and east when ballooning crews were operating. Initial echo tops were approximately 4 km AGL before 1200 UTC, while the band was still well organized. An environmental sounding in Oswego at 1230 UTC showed the boundary layer reaching 500 hPa. The in situ balloon crew deployed along the lakeshore north of Scriba, New York (see Fig. 1 for location), west-northwest of the DOW7 location. Limited in situ observation sets were available for launch after the previous IOP, so only a single EFM was launched at 1655 UTC when the LeS band was more cellular but producing mixed graupel and dendrites at the location. Again, a similar +/−/+ charge structure was observed (not shown). However, by launch time

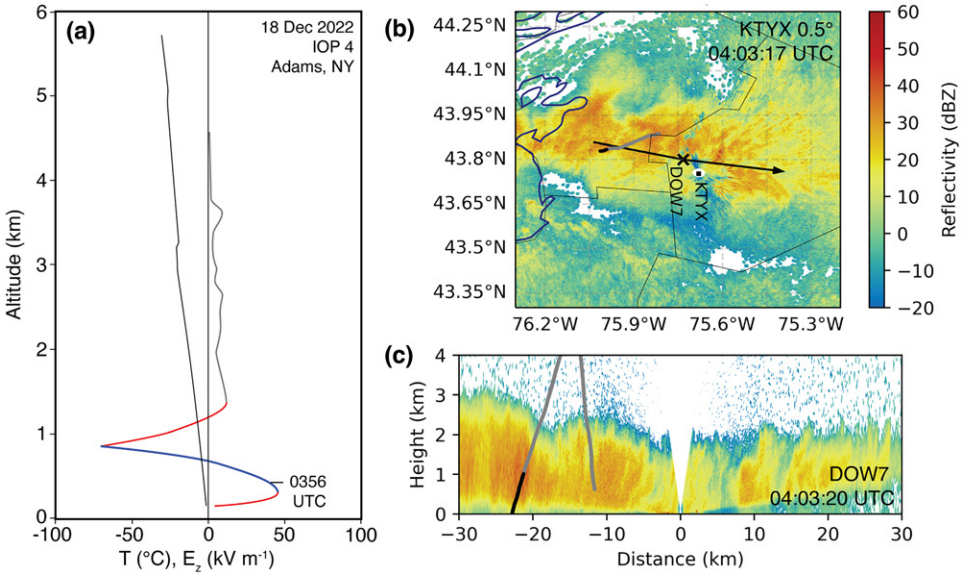

Fig. 6. Observations from IOP4 on 18 Dec 2022. (a) Vertical profile of temperature and a manually smoothed, signed magnitude of the electric field as in Fig. 4, launched at 0356 UTC near Adams, New York (location in Fig. 1). (b) Plan view of KTYX radar reflectivity at 0.5° elevation angle beginning 0403:17 UTC. The map shows counties in New York (black lines) and Lake Ontario (blue line). (c) Vertical cross section of DOW7 radar reflectivity beginning 0403:20 UTC, with the radar at the x in (b). Black arrow in (b) indicates the azimuth and increasing distance of the cross section in (c). Gray line in (b) and (c) is the trajectory of the balloon in (a), with the portion of the path before the radar scans in black.

when what remained of the band reached the southern sample axis, the echo top heights had decreased to approximately 2.5 km AGL. The flashes which had been observed over the Tug Hill during event 5 ceased by 0800 UTC 19 December, before the band reached the IOP5 deployment area, making IOP5 another null case bookending the electrically active period of event 5. Each of IOP4 and IOP5 had similar charge structures in their soundings into the bands on the opposite sides of the Tug Hill, but echo tops only reached 4 km AGL at maximum. Given the decay in heights noted at the start of IOP5, it is suspected that the charged volumes were not sufficiently deep or organized enough in either of the IOPs to generate the electric fields necessary to produce lightning flashes within them but were deep enough between the two periods (event 5).

5. Processes and phenomena

a. Conceptual model of electrification in lake-effect storms. A conceptual model of lightning and electrification structure in LeSs based on LEE observations is summarized in Fig. 7. Consistent with the EFM profiles launched in active convective cells forced by the warm lake surface, and the few nearshore lightning discharges we observed, three charge layers are indicated near shore. Each EFM profile (with electric field magnitude greater than tens of kilovolts per m) showed positive charge immediately above the surface with a depth of no more than 1000 m, and with a relatively large charge density, on the order of 1 nC m^{-3}, usually matching or exceeding the negative charge density above it. The very shallow tripole observed during IOP4 (Fig. 6a) had all three charge layers at temperatures between 0° and −10°C, likely requiring an electrification polarity reversal temperature of about −5°C at relatively low liquid water contents.

Further inland, as the shallow layer of positive charge carried on graupel precipitated out of the system, a dipole remains: Positive charge carried on ice crystals aloft, while precipitating graupel and snow carried net-negative charge. The upper portion of the EFM profiles was also consistent with the presence of the upper two charge layers, showing positive charge below cloud top and negative charge below the positive charge.

The nearshore positive graupel probably fell out within tens of kilometers of shore, while the negative graupel extends up to 50 km inland (consistent with observations at the LEE DOW7 sites). The precise location of the transition from nearshore positive charge to inland negative charge near the surface remains unclear. We suspect that it is primarily driven by

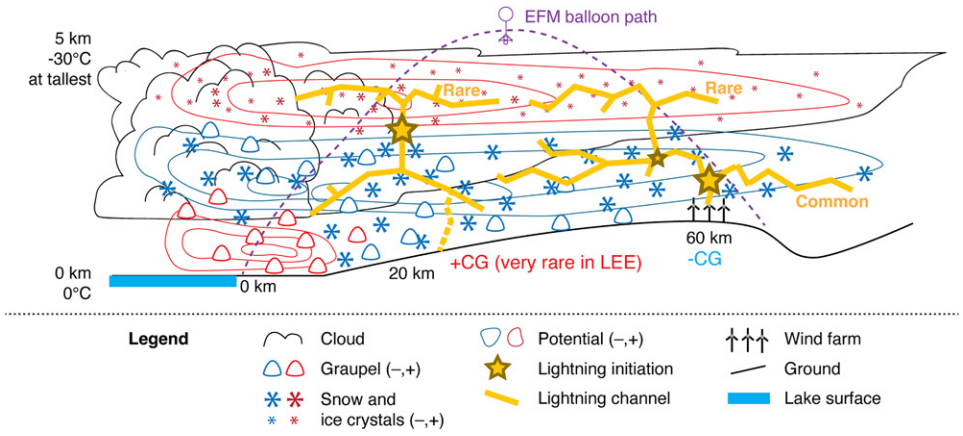

Fig. 7. Conceptual model of electrical structure in lake-effect snow in vertical cross section. The legend indicates the meaning of symbols. Distances along the ground are relative to the lakeshore, with the cloud transitioning from cumuliform to stratiform with distance. Charge is indicated on ice crystals, snow, and graupel, which produce regions of electrical potential, with lightning initiation in regions of large electric fields. A small yellow star depicts the location of the secondary development of negative leaders into the upper positive charge after the initial development of positive leaders into negative charge from the towers.

enhanced graupel growth rates in the most intense convective cells, which subside inland as the instability from the warm lake is consumed. It is not clear if the terrain specific to our field campaign plays a role in preventing positive charge farther inland.

Our assignment of charge to certain hydrometeor species is supported by examining observations from the PASIV both visually and through an automated detection algorithm. Preliminary processing of the PASIV data indicates the presence of graupel at lower altitudes (<1 km in the IOP10 sounding) which transitions to more aggregate and branched structures above that altitude. Further refinement and comparison with the EFM data are needed to place the particle observations within the observed electric field to determine bulk charge likely present, but in general, the observations from the PASIV support the conceptual model.

As nearshore convective cells transition into a more stratiform precipitating band, more horizontally extensive charge regions are found near the ground and can directly enhance the electric field and support initiation of lightning at any of the wind turbines or other tall towers in the vicinity. Upward discharges from the towers in LEE had positive leaders, also implying negative charge near the surface. Occasionally, the tower-initiated discharges also exhibited a higher-altitude layer of negative leaders moving into positive charge in the upper portion of the cloud, as in Schultz et al. (2018). For consistency with prior measurements, we include positive CGs in Fig. 7, even though only three, with high classification uncertainty, were observed by the ENTLN during LEE.

Steiger et al. (2018; Fig. 19) summarized the electrical structure of LeSs as only dipolar, so the finding of positive charge on graupel near shore is a revision to the earlier model of lake-effect snow. However, recent measurements in Japanese sea-effect snow (Takahashi et al. 2019; Zheng et al. 2019) also showed a lower positive charge layer. Future work will be able to use EFM and thermodynamic and microphysical data from all balloon flights to test our understanding of fundamental electrification microphysics by carefully considering the reversal temperature and associated microphysical growth regimes.

b. Simulating the electrical nature of lake-effect storms. Accurately modeling storm electrification has uncertainties, particularly because the simulated electrification is sensitive to the microphysical populations and electrical parameterizations (Mansell et al. 2005; Fierro et al. 2006; Blair 2021). The observation sets in the Project LEE provide a unique opportunity to investigate how well electrification numerical modeling performs in lake-effect thunderstorms. We conducted a WRF convection-permitting simulation of IOP2, driven by the ERA5 reanalysis. The outer and inner domains of this simulation are resolved by horizontal gridcell spacings of 9 and 3 km, respectively. The outer domain covered the Midwest, northeast, and south regions of the continental United States and the southern part of Canada that allows the model to simulate synoptic weather systems. The inner domain is centered on the region surrounding Lake Ontario and covers Lakes Huron and Erie. The WRF Model v4.2.2 was configured with the NSSL 2-moment microphysical scheme (Ziegler 1985; Mansell et al. 2010), the Mellor–Yamada–Janjić planetary boundary layer scheme (Mellor and Yamada 1982; Janjić 2001), the Rapid Radiative Transfer Model for GCMs (RRTMG) shortwave and longwave radiation scheme (Iacono et al. 2008), and the Noah land surface scheme (Chen and Dudhia 2001; Ek et al. 2003). The lightning potential index (LPI) lightning scheme was adopted to predict the potential of lightning activity (Yair et al. 2010). The simulated LPI is the kinetic energy from the updraft in the developing convective cloud with a unit of joules per kilogram (J kg^{-1}).

Results from the simulation were verified against the EFM sounding at 2300 UTC 18 November 2022 and the nearby KTYX (Fort Drum, New York) NEXRAD radar data. The simulated sounding was able to reproduce the deep saturated layer up to 500 hPa as observed

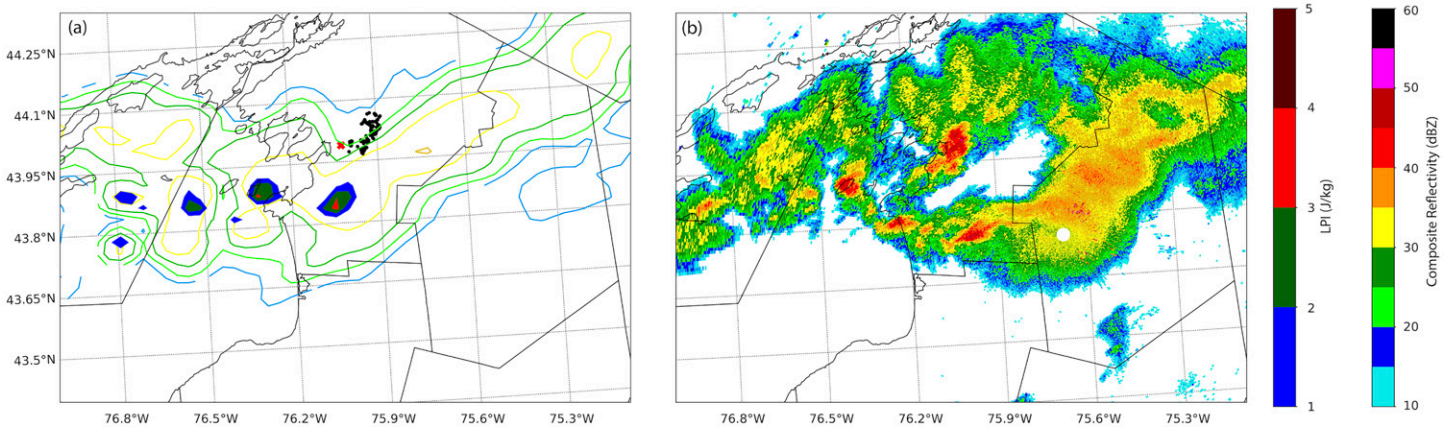

Fig. 8. (a) WRF-simulated LPI at 0000 UTC 19 Nov 2022 depicted together with a lightning flash detected by the LMA (black dots) from 0010 to 0020 UTC 19 Nov 2022. The red cross represents the location where lightning was visually observed by the DOW7 operators. The contour lines are WRF-simulated composite reflectivity at 0000 UTC 19 Nov 2022. (b) KTYX composite radar reflectivity at 0000 UTC 19 Nov 2022.

in the EFM sounding (Fig. 4a). The simulation shows the development of a LLAP band over eastern Lake Ontario on 18 November. This band then continued to develop over Lake Ontario while shifting a few kilometers north. The values of model simulated composite reflectivity were reasonably comparable to the observed values, and the location of the LLAP band from the simulation agrees well with the band location from radar observations (Fig. 8).

The LPI from the simulation is used to assess the location and likelihood of lake-effect lightning. LPI values up to 5 J kg^{-1} on the eastern shore of Lake Ontario near Watertown at 0000 UTC 19 November indicate the intense convection in the LLAP band (Fig. 8). By comparison, Yair et al. (2010) found that forecast LPI values ranging from 1 to above 20 J kg^{-1} were associated with lightning productions in Mediterranean storms. The general similarity between the simulated LPI and the observed lightning flash from the LMA and DOW7 operators (Fig. 8) suggests that LPI can be used as an effective predictor of lake-effect lightning. It should be noted that there is a southward displacement between the simulated LPI and the observed flashes.

Another modeling study is currently in progress which conducts a simulation of IOP2 using the WRF-electrification model (Fierro et al. 2013). The simulated charge regions will be compared with those observed from EFMs and inferred charge regions from the LMA to provide insight into the physical processes relevant to the initiation of lake-effect lightning.

6. Education and outreach

a. Forecasting. Project LEE provided a unique experience for SUNY Oswego undergraduate students. For many, it was their first time participating in an organized research project. Students were also an integral part in the daily forecasting process for LEE operations. The forecasting team was composed of two Oswego undergraduates and two professors. Student forecasters were able to continuously improve their skill and communication while forecasting throughout the project. Daily hybrid (in person + online via Zoom) briefings served to communicate these forecasts and confidence on potential IOPs to PIs and scientists. These briefings consisted of forecasts by the National Weather Service Buffalo or Albany followed by the student forecasters. Each began with the short-range (next 1–3 days) outlook of lake-effect and electrification potential followed by a longer-range forecast for conducive weather patterns beyond 72 h.

b. Involvement of undergraduate students in the field. In addition to providing invaluable forecasts, undergraduate students were instrumental in completing the field phase of the

project. For each IOP, 8–16 students (depending on whether there were one or two ballooning teams) were assigned to help with the EFM launches and two were assigned to assist the DOW7 team. Students on balloon teams drove vehicles, assisted in preparing and launching the instruments, helped with nowcasting during operations, and took snowfall measurements during IOPs. Students on the DOW7 team aided communications between the other teams and the DOW7 operators, cleared snow from around the radar, and collected snowfall measurements. The students were eager to help with every aspect of the project, including retrieving instruments after launch and shoveling snow at LMA stations to keep them powered. Students also volunteered in the laboratory to help with the building, troubleshooting, and calibration of instruments. This gave the students an inside look into how senior scientists problem solve and innovate in the laboratory and in the field, often with whatever tools are readily available. These roles are critical in fieldwork efforts, and the Project LEE gave the students a chance to gain experience in those roles. Details of the undergraduate students' experiences during IOPs can be found in the "Student field experiences" sidebar.

c. Outreach to the central New York community. The communities in and around the Tug Hill were quite welcoming and interested in the Project LEE. Katie Malinowski, executive director of the New York State Tug Hill Commission, invited S. Steiger (SUNY Oswego) to present to the Commission in August and September 2022. Several local residents at these meetings expressed interest in helping by donating the use of their land for LMA sensor placement. Residents also gave a list of contacts for snowmobilers who could help retrieve EFM sondes in the Tug Hill forests. During the field campaign, local snowplow operators volunteered to assist some of the mobile sounding team vehicles that got stuck in deep snow. A couple of other examples of local interest in the project included Jay Matteson's Rural America podcast interviews with S. Steiger and the friendliness of the Watertown International Airport personnel (Grant Sussey et al.), who gave Project LEE participants a tour of the facilities during visits to clean snow off the LMA unit and allowed for operation of DOW7 on airport grounds.

An open house for the public occurred on 5 November 2022 at the Shineman Science Center of SUNY Oswego. DOW7, a mesonet vehicle, LMA sensor, and EFM sondes were shown by the scientists to ~100 guests, some of whom were also attendees to the Great Lakes Atmospheric Science Symposium, a regional conference hosted by the SUNY Oswego Meteorology Club at the Shineman Center the same day.

Several K–12 educational visits occurred during the project. DOW7, along with several Oswego undergraduates and the NSSL LMA crew, visited with multiple classes in the Oswego and Camden, New York, school districts.

7. Conclusions

The LEE field project collected unprecedented data on the microphysics and electrification in LeSs. Some key aspects of the fieldwork include the following:

- First of their kind, EFM and LMA observations have already helped us revise our basic conceptual model of the electrical structure of LeSs, with a nearshore tripole with lower positive charge, and upward discharges into negative charge from man-made structures on the Tug Hill, confirming results from the OWLeS Project. Some LEE results may also lead to revisions in how the sign and magnitude of hydrometeor charging depend on the microphysical environment.
- Over one-third (33%, a lower bound) of LEE LMA lightning flashes were associated with man-made towers, and the lake-effect lightning "hot spots" occurred over wind turbine fields east of Lake Ontario showing more work needs to be done to mitigate damages from this kind of lightning.

Student field experiences

Throughout the Project LEE field campaign, 22 Oswego undergraduate students (several first year) gained valuable research experience by assisting with field tasks led by senior scientists. Across forecasting, sounding, and DOW7 teams, students had varied experiences and made additional contributions beyond those planned. (See the Education and Outreach section for more details of contributions the students made during the project.) Working alongside senior scientists provided students with unique opportunities to observe, experience, and learn about weather and the practical realities of fieldwork.

Several interesting meteorological phenomena were observed throughout the field campaign. During IOP3 (20 November 2022), one of the student forecasters captured a video of a lightning flash striking one of the Oswego, New York, Harbor Power stacks (see supplemental video), as well as several students photographing and describing the large (nearly 2 cm) and conical-shaped graupel that fell from the band (Fig. SB1). The sounding team was in the heart of the lake-effect band in Henderson, New York, during IOP10 (1–2 February 2023) and measured 2.4 in. (6.1 cm) of snowfall in 1 h, which was the heaviest snowfall ever experienced by many of these students! During IOP11 (2–3 February 2023), the students on the DOW7 team visually observed 20 lightning flashes while located on the Tug Hill, which later proved very helpful during data analysis since only half of the original LMA stations were operational, likely causing the LMA network to detect fewer flashes.

Fig. SB1. Photo of large [0.75 in. (1.9 cm) diameter] conical graupel during LEE IOP3 (20 Nov 2022). (Photo courtesy of J. Rumowicz.)

Stress relief is an important aspect of field research, as sometimes long hours of staying out in the field are required to collect desirable data. During IOP4 (17–18 December 2022), the sounding and the DOW7 teams were in the field throughout the night waiting for the band to shift southward—an event delayed several hours later than forecast. To fill time and help alleviate the stress of staying out in the cold, sheltered inside a running vehicle all night, the sounding team had fun by playing kickball in a snowy field, while the DOW7 team enjoyed a pizza party (delivered) inside the truck. During IOP6 (24 January 2023), while waiting for a narrow, yet intense band to move over the stationed locations, one of the sounding teams deployed at Fort Ontario (Oswego) and was given a tour of the historical site by one of the caretakers, as well as learned about the coastal storm flag warning station located at the fort (where the lake-effect band warranted a flag to be staffed that day).

Spending time with senior scientists also provided opportunities for impromptu science lessons. For example, during downtime during IOP2 one of the senior scientists made a snowball the approximate size (20 cm) of the world-record-setting hailstone (Pojorlie et al. 2013; Kumjian et al. 2020) and went on to give the students a summary of how a hailstone of that magnitude can be generated by a thunderstorm updraft. Overall, the students had a well-rounded experience of learning about fieldwork, instrumentation, and general meteorology while participating in the Project LEE.

- We completed the campaign in challenging conditions, with excellent undergraduate forecast support and field involvement. The central and northern New York communities were also very interested in helping with the LEE field project, volunteering time and land space, and offering several opportunities to present about the project.

- Lessons learned from this first effort prove the value of making balloon in situ measurements in LeSs and will help us design future experiments targeted at understanding microphysics, electrification, and lightning in the unique mixed-phase natural laboratory that is LeS and other winter storms.

Acknowledgments. We greatly appreciate the participation of 24 undergraduates (Aidan Alwang, Joseph Berry, Evan Biedron, Zoe Bush, Ezekiel Caldon, Thomas Cerra, Kristina Foster, Max Gallo, Sarah Gryskewicz, Daniel Hummel, Kaitlyn Jesmonth, Samantha Karlsson, Erik Knudsen, Shaun Laurinaitis, Kayla Lewis, Christopher Luft, Michael Pagnanelli, Josephine Ragland, Jake Rumowicz, Brianna Saunders, Christopher Schneider, Garrett Statum, Thomas Weist, and Thomas White), graduate students (Jessica Souza, David Singewald, and Matthew Miller), and postdoctoral scholars (Kelcy Brunner, Jacquelyn Ringhausen, and Vicente Salinas) in collecting data and weather forecasters at the Buffalo and Albany NOAA/NWS Forecast Offices. Particular thanks go to David Zaff who organized the daily NWS forecast discussions. We thank the New York Tug Hill Commission (especially executive director Katie Malinowski) for helping us find landowner contact information for balloon retrievals, as well as Jay Matteson, the Jefferson County Agricultural Coordinator, Dustin Hite with the Osceola Ski and Sport Resort, Emily and Chris with Tug Hill Outfitters for their assistance in identifying instrumentation sites, and all those who donated their property for this purpose. LEE was funded by the National Science Foundation, Grants NSF AGS 2212177 (SUNY Oswego), 2113207 (University of Illinois), 2212199 (University of Oklahoma), 2212184 (Georgia Tech Applied Research Corporation), 2212227 (Texas Tech University), and 2212196 (University of Alabama Huntsville), the NOAA/OAR National Severe Storms Laboratory, and NOAA/Office of Oceanic and Atmospheric Research under NOAA–University of Oklahoma Cooperative Agreement NA21OAR4320204, U.S. Department of Commerce. Thanks to SUNY Oswego for hosting research labs and the operation center where scientists were able to work on instrumentation and have discussions.

Data availability statement. We would like to acknowledge operational, technical, and scientific support including the Field Catalog (https://doi.org/10.5065/D6SQ8XFB), the Field Data Archive (https://data.eol.ucar.edu/master_lists/generated/lee/), and related staffing support provided by NCAR's Earth Observing Laboratory, sponsored by the National Science Foundation. LEE data are publicly available per the LEE Data Policy available at https://www.eol.ucar.edu/field_projects/lee. Radar images were produced using Py-ART (Helmus and Collis 2016). DOW data are also accessible from Wurman and Kosiba (2023).

References

Avila, E. E., C. P. R. Saunders, H. Bax-Norman, and N. E. Castellano, 2005: Charge sign reversal in irregular ice particle-graupel collisions. *Geophys. Res. Lett.*, **32**, L01801, https://doi.org/10.1029/2004GL020761.

Baker, B., M. B. Baker, E. R. Jayaratne, J. Latham, and C. P. R. Saunders, 1987: The influence of diffusional growth rates on the charge transfer accompanying rebounding collisions between ice crystals and soft hailstones. *Quart. J. Roy. Meteor. Soc.*, **113**, 1193–1215, https://doi.org/10.1002/qj.49711347807.

Blair, J. F., 2021: Modeling CCN effects in electrification within high and low precipitation supercells. Ph.D. thesis, University of Oklahoma, 128 pp., https://hdl.handle.net/11244/330165.

Brook, M., M. Nakano, P. Krehbiel, and T. Takeuti, 1982: The electrical structure of the Hokuriku winter thunderstorms. *J. Geophys. Res.*, **87**, 1207–1215, https://doi.org/10.1029/JC087iC02p01207.

Bruning, E. C., S. A. Weiss, and K. M. Calhoun, 2014: Continuous variability in thunderstorm primary electrification and an evaluation of inverted-polarity terminology. *Atmos. Res.*, **135–136**, 274–284, https://doi.org/10.1016/j.atmosres.2012.10.009.

Chen, F., and J. Dudhia, 2001: Coupling an advanced land surface–hydrology model with the Penn State–NCAR MM5 modeling system. Part I: Model implementation and sensitivity. *Mon. Wea. Rev.*, **129**, 569–585, https://doi.org/10.1175/1520-0493(2001)129<0569:CAALSH>2.0.CO;2.

Chmielewski, V., Z. Barney, K. Calhoun, D. Kennedy, J. Ringhausen, V. Salinas, and M. Stock, 2023: NSSL deployable lightning mapping array data. NOAA/OAR National Severe Storms Laboratory, https://doi.org/10.15763/DBS.DLMA.

Chmielewski, V. C., and E. C. Bruning, 2016: Lightning mapping array flash detection performance with variable receiver thresholds. *J. Geophys. Res. Atmos.*, **121**, 8600–8614, https://doi.org/10.1002/2016JD025159.

Coleman, L. M., T. C. Marshall, M. Stolzenburg, T. Hamlin, P. R. Krehbiel, W. Rison, and R. J. Thomas, 2003: Effects of charge and electrostatic potential on lightning propagation. *J. Geophys. Res.*, **108**, 4298, https://doi.org/10.1029/2002JD002718.

Dye, J. E., and A. Bansemer, 2019: Electrification in mesoscale updrafts of deep stratiform and anvil clouds in Florida. *J. Geophys. Res. Atmos.*, **124**, 1021–1049, https://doi.org/10.1029/2018JD029130.

Ek, M. B., K. E. Mitchell, Y. Lin, E. Rogers, P. Grummann, V. Koren, G. Gayno, and J. D. Tarpley, 2003: Implementation of Noah land surface model advances in the National Centers for Environmental Prediction operational mesoscale Eta model. *J. Geophys. Res.*, **108**, 8851, https://doi.org/10.1029/2002JD003296.

Emersic, C., and C. P. R. Saunders, 2010: Further laboratory investigations into the Relative Diffusional Growth Rate theory of thunderstorm electrification. *Atmos. Res.*, **98**, 327–340, https://doi.org/10.1016/j.atmosres.2010.07.011.

Fierro, A. O., M. S. Gilmore, E. R. Mansell, L. J. Wicker, and J. M. Straka, 2006: Electrification and lightning in an idealized boundary-crossing supercell simulation of 2 June 1995. *Mon. Wea. Rev.*, **134**, 3149–3172, https://doi.org/10.1175/MWR3231.1.

——, E. R. Mansell, D. R. MacGorman, and C. L. Ziegler, 2013: The implementation of an explicit charging and discharge lightning scheme within the WRF-ARW model: Benchmark simulations of a continental squall line, a tropical cyclone, and a winter storm. *Mon. Wea. Rev.*, **141**, 2390–2415, https://doi.org/10.1175/MWR-D-12-00278.1.

Glassmeier, F., L. Arnold, R. Dietlicher, M. Paukert, and U. Lohmann, 2018: A modeling study on the sensitivities of atmospheric charge separation according to the relative diffusional growth rate theory to nonspherical hydrometeors and cloud microphysics. *J. Geophys. Res. Atmos.*, **123**, 12 236–12 252, https://doi.org/10.1029/2018JD028356.

Goodman, S. J., and Coauthors, 2013: The GOES-R Geostationary Lightning Mapper (GLM). *J. Atmos. Res.*, **125–126**, 34–49, https://doi.org/10.1016/j.atmosres.2013.01.006.

Harkema, S. S., E. B. Berndt, and C. J. Schultz, 2020: Characterization of snowfall rates, totals, and snow-to-liquid ratios in electrified snowfall events identified by the Geostationary Lightning Mapper. *Wea. Forecasting*, **35**, 673–689, https://doi.org/10.1175/WAF-D-19-0126.1.

Helmus, J. J., and S. M. Collis, 2016: The Python ARM Radar Toolkit (Py-ART), a library for working with weather radar data in the Python programming language. *J. Open Res. Software*, **4**, 25, https://doi.org/10.5334/jors.119.

Hoen, B. D., J. E. Diffendorfer, J. T. Rand, L. A. Kramer, C. P. Garrity, and H. E. Hunt, 2018: United States Wind Turbine Database v6.1 (November 28, 2023). USGS, American Clean Power Association, and Lawrence Berkeley National Laboratory data release, accessed 30 October 2023, https://doi.org/10.5066/F7TX3DN0.

Iacono, M. J., J. S. Delamere, E. J. Mlawer, M. W. Shephard, S. A. Clough, and W. D. Collins, 2008: Radiative forcing by long-lived greenhouse gases: Calculations with the AER radiative transfer models. *J. Geophys. Res.*, **113**, D13103, https://doi.org/10.1029/2008JD009944.

Illingworth, A. J., and J. Latham, 1977: Calculations of electric field growth, field structure and charge distributions in thunderstorms. *Quart. J. Roy. Meteor. Soc.*, **103**, 281–295, https://doi.org/10.1002/qj.49710343606.

Janjić, Z. I., 2001: Nonsingular implementation of the Mellor-Yamada level 2.5 scheme in the NCEP Meso model. NOAA/NWS/NCEP Office Note 437, 61 pp.

Jayaratne, E. R., C. P. R. Saunders, and J. Hallett, 1983: Laboratory studies of the charging of soft-hail during ice crystal interactions. *Quart. J. Roy. Meteor. Soc.*, **109**, 609–630, https://doi.org/10.1002/qj.49710946111.

Kingfield, D. M., K. M. Calhoun, and K. M. de Beurs, 2017: Antenna structures and cloud-to-ground lightning location: 1995–2015. *Geophys. Res. Lett.*, **44**, 5203–5212, https://doi.org/10.1002/2017GL073449.

Kitagawa, N., and K. Michimoto, 1994: Meteorological and electrical aspects of winter thunderclouds. *J. Geophys. Res.*, **99**, 10 713–10 721, https://doi.org/10.1029/94JD00288.

Kristovich, D. A. R., and Coauthors, 2017: The Ontario Winter Lake-effect Systems field campaign: Scientific and educational adventures to further our knowledge and prediction of lake-effect storms. *Bull. Amer. Meteor. Soc.*, **98**, 315–332, https://doi.org/10.1175/BAMS-D-15-00034.1.

Kumjian, M. R., and Coauthors, 2020: Gargantuan hail in Argentina. *Bull. Amer. Meteor. Soc.*, **101**, E1241–E1258, https://doi.org/10.1175/BAMS-D-19-0012.1.

Letcher, T., and S. Steiger, 2010: Lake-effect climatology of the Great Lakes. *Natl. Wea. Dig.*, **34**, 158–168.

Luque, M. Y., R. Burgesser, and E. Ávila, 2016: Thunderstorm graupel charging in the absence of supercooled water droplets. *Quart. J. Roy. Meteor. Soc.*, **142**, 2418–2423, https://doi.org/10.1002/qj.2834.

MacGorman, D. R., and W. D. Rust, 1998: *The Electrical Nature of Storms.* Oxford University Press, 422 pp.

——, and Coauthors, 2008: TELEX the Thunderstorm Electrification and Lightning Experiment. *Bull. Amer. Meteor. Soc.*, **89**, 997–1014, https://doi.org/10.1175/2007BAMS2352.1.

Mansell, E. R., D. R. MacGorman, C. L. Ziegler, and J. M. Straka, 2005: Charge structure and lightning sensitivity in a simulated multicell thunderstorm. *J. Geophys. Res.*, **110**, D12101, https://doi.org/10.1029/2004JD005287.

——, C. L. Ziegler, and E. C. Bruning, 2010: Simulated electrification of a small thunderstorm with two-moment bulk microphysics. *J. Atmos. Sci.*, **67**, 171–194, https://doi.org/10.1175/2009JAS2965.1.

Market, P. S., and A. E. Becker, 2009: A study of lightning flashes attending periods of banded snowfall. *Geophys. Res. Lett.*, **36**, L01809, https://doi.org/10.1029/2008GL036317.

——, and Coauthors, 2006: Proximity soundings of thundersnow in the central United States. *J. Geophys. Res.*, **111**, D19208, https://doi.org/10.1029/2006JD007061.

McMurdie, L. A., and Coauthors, 2022: Chasing snowstorms: The Investigation of Microphysics and Precipitation for Atlantic Coast-Threatening Snowstorms (IMPACTS) campaign. *Bull. Amer. Meteor. Soc.*, **103**, E1243–E1269, https://doi.org/10.1175/BAMS-D-20-0246.1.

Mellor, G. L., and T. Yamada, 1982: Development of a turbulence closure model for geophysical fluid problems. *Rev. Geophys.*, **20**, 851–875, https://doi.org/10.1029/RG020i004p00851.

Montanyà, J., O. van der Velde, and E. R. Williams, 2014: Lightning discharges produced by wind turbines. *J. Geophys. Res. Atmos.*, **119**, 1455–1462, https://doi.org/10.1002/2013JD020225.

Moore, P. K., and R. E. Orville, 1990: Lightning characteristics in lake-effect thunderstorms. *Mon. Wea. Rev.*, **118**, 1767–1782, https://doi.org/10.1175/1520-0493(1990)118<1767:LCILET>2.0.CO;2.

Murphy, M. J., J. A. Cramer, and R. K. Said, 2021: A recent history of upgrades to the U.S. National Lightning Detection Network. *J. Atmos. Oceanic Technol.*, **38**, 573–585, https://doi.org/10.1175/JTECH-D-19-0215.1.

NCEI, 2023: Data access. Accessed 19 December 2023, https://www.ncei.noaa.gov/access/search/index.

Niziol, T. A., W. R. Snyder, and J. S. Waldstreicher, 1995: Winter weather forecasting throughout the eastern United States. Part IV: Lake effect snow. *Wea. Forecasting*, **10**, 61–77, https://doi.org/10.1175/1520-0434(1995)010<0061:WWFTTE>2.0.CO;2.

Pojorlie, K. L., S. Doering, and M. A. Fowle, 2013: The record-breaking Vivian, South Dakota hailstorm of 23 July 2010. *J. Oper. Meteor.*, **1**, 3–18, https://doi.org/10.15191/nwajom.2013.0102.

Rauber, R. M., and Coauthors, 2014: Stability and charging characteristics of the comma head region of continental winter cyclones. *J. Atmos. Sci.*, **71**, 1559–1582, https://doi.org/10.1175/JAS-D-13-0253.1.

Rust, W. D., and Coauthors, 2005: Inverted-polarity electrical structures in thunderstorms in the Severe Thunderstorm Electrification and Precipitation Study (STEPS). *Atmos. Res.*, **76**, 247–271, https://doi.org/10.1016/j.atmosres.2004.11.029.

Saunders, C. P. R., H. Bax-Norman, C. Emersic, E. E. Avila, and N. E. Castellano, 2006: Laboratory studies of the effect of cloud conditions on graupel/crystal charge transfer in thunderstorm electrification. *Quart. J. Roy. Meteor. Soc.*, **132**, 2653–2673, https://doi.org/10.1256/qj.05.218.

Schultz, C. J., W. A. Petersen, and L. D. Carey, 2011: Lightning and severe weather: A comparison between total and cloud-to-ground lightning trends. *Wea. Forecasting*, **26**, 744–755, https://doi.org/10.1175/WAF-D-10-05026.1.

——, T. J. Lang, E. C. Bruning, K. M. Calhoun, S. Harkema, and N. Curtis, 2018: Characteristics of lightning within electrified snowfall events using lightning mapping arrays. *J. Geophys. Res. Atmos.*, **123**, 2347–2367, https://doi.org/10.1002/2017JD027821.

Schuur, T. J., W. D. Rust, B. F. Smull, and T. C. Marshall, 1991: Electrical and kinematic structure of the stratiform precipitation region trailing an Oklahoma squall line. *J. Atmos. Sci.*, **48**, 825–842, https://doi.org/10.1175/1520-0469(1991)048<0825:EAKSOT>2.0.CO;2.

Smith, W. H. F., and D. T. Sandwell, 1997: Global seafloor topography from satellite altimetry and ship depth soundings. *Science*, **277**, 1957–1962, https://doi.org/10.1126/science.277.5334.1956.

Steiger, S. M., R. Hamilton, J. Keeler, and R. E. Orville, 2009: Lake-effect thunderstorms in the lower Great Lakes. *J. Appl. Meteor. Climatol.*, **48**, 889–902, https://doi.org/10.1175/2008JAMC1935.1.

——, and Coauthors, 2013: Circulations, bounded weak echo regions, and horizontal vortices observed within long-lake-axis-parallel–lake-effect storms by the Doppler on Wheels. *Mon. Wea. Rev.*, **141**, 2821–2840, https://doi.org/10.1175/MWR-D-12-00226.1.

——, T. Kranz, and T. W. Letcher, 2018: Thunderstorm characteristics during the Ontario Winter Lake-Effect Systems project. *J. Appl. Meteor. Climatol.*, **57**, 853–874, https://doi.org/10.1175/JAMC-D-17-0188.1.

Stough, S. M., L. D. Carey, C. J. Schultz, and P. M. Bitzer, 2017: Investigating the relationship between lightning and mesocyclonic rotation in supercell thunderstorms. *Wea. Forecasting*, **32**, 2237–2259, https://doi.org/10.1175/WAF-D-17-0025.1.

Stucke, I., D. Morgenstern, G. Diendorfer, G. J. Mayr, H. Pichler, W. Schulz, T. Simon, and A. Zeileis, 2023: Upward lightning at the Gaisberg Tower: The larger-scale meteorological influence on the triggering mode and flash type. *J. Geophys. Res. Atmos.*, **128**, e2022JD037776, https://doi.org/10.1029/2022JD037776.

Takahashi, T., 1978: Riming electrification as a charge generation mechanism in thunderstorms. *J. Atmos. Sci.*, **35**, 1536–1548, https://doi.org/10.1175/1520-0469(1978)035<1536:REAACG>2.0.CO;2.

——, S. Sugimoto, T. Kawano, and K. Suzuki, 2019: Microphysical structure and lightning initiation in Hokuriku winter clouds. *J. Geophys. Res. Atmos.*, **124**, 13 156–13 181, https://doi.org/10.1029/2018JD030227.

U.S. Census Bureau, 2019: TIGER/Line Shapefiles: Roads: Primary and secondary roads. Accessed 30 October 2023, https://www.census.gov/cgi-bin/geo/shapefiles/index.php?year=2019&layergroup=Roads.

Wang, D., N. Takagi, T. Watanabe, H. Sakurano, and M. Hashimoto, 2008: Observed characteristics of upward leaders that are initiated from a windmill and its lightning protection tower. *Geophys. Res. Lett.*, **35**, L02803, https://doi.org/10.1029/2007GL032136.

Warner, T. A., K. L. Cummins, and R. E. Orville, 2012: Upward lightning observations from towers in Rapid City, South Dakota and comparison with National Lightning Detection Network data, 2004–2010. *J. Geophys. Res.*, **117**, D19109, https://doi.org/10.1029/2012JD018346.

Waugh, S. M., C. L. Ziegler, D. R. MacGorman, S. E. Fredrickson, D. W. Kennedy, and W. D. Rust, 2015: A balloonborne Particle Size, Imaging, and Velocity probe for in situ microphysical measurements. *J. Atmos. Oceanic Technol.*, **32**, 1562–1580, https://doi.org/10.1175/JTECH-D-14-00216.1.

Williams, E., V. Mushtak, D. Rosenfeld, S. Goodman, and D. Boccippio, 2005: Thermodynamic conditions favorable to superlative thunderstorm updraft, mixed phase microphysics and lightning flash rate. *Atmos. Res.*, **76**, 288–306, https://doi.org/10.1016/j.atmosres.2004.11.009.

Wurman, J., and K. Kosiba, 2023: Lake-Effect Electrification (LEE) Flexible Array of Radars and Mesonets (FARM) Doppler on Wheels (DOW) data, version 1. FARM, https://doi.org/10.48514/8NK8-NE59.

——, and Coauthors, 2021: The Flexible Array of Radars and Mesonets (FARM). *Bull. Amer. Meteor. Soc.*, **102**, E1499–E1525, https://doi.org/10.1175/BAMS-D-20-0285.1.

Yair, Y., B. Lynn, C. Price, V. Kotroni, K. Lagouvardos, E. Morin, A. Mugnai, and M. C. Llasat, 2010: Predicting the potential for lightning activity in Mediterranean storms based on the Weather Research and Forecasting (WRF) model dynamic and microphysical fields. *J. Geophys. Res.*, **115**, D04205, https://doi.org/10.1029/2008JD010868.

Zheng, D., D. Wang, Y. Zhang, T. Wu, and N. Takagi, 2019: Charge regions indicated by LMA lightning flashes in Hokuriku's winter thunderstorms. *J. Geophys. Res. Atmos.*, **124**, 7179–7206, https://doi.org/10.1029/2018JD030060.

Zhu, Y., M. Stock, J. Lapierre, and E. DiGangi, 2022: Upgrades of the Earth Networks Total Lightning Network in 2021. *Remote Sens.*, **14**, 2209, https://doi.org/10.3390/rs14092209.

Ziegler, C. L., 1985: Retrieval of thermal and microphysical variables in observed convective storms. Part I: Model development and preliminary testing. *J. Atmos. Sci.*, **42**, 1487–1509, https://doi.org/10.1175/1520-0469(1985)042<1487:ROTAMV>2.0.CO;2.